Journal of Power Sources 321 (2016) 126–134

Contents lists available at ScienceDirect

Journal of Power Sources

journal homepage: www.elsevier.com/locate/jpowsour

The impact of pH on side reactions for aqueous redox flow batteries based on nitroxyl radical compounds

A. Orita [a, b], M.G. Verde [a], M. Sakai [b], Y.S. Meng [a, *]

[a] Department of NanoEngineering, University of California, San Diego, 9500 Gilman Drive, La Jolla, CA 92093, USA
[b] Tsukuba Research Laboratory, Hitachi Chemical, 48 Wadai, Tsukuba-shi, Ibaraki 300-4247, Japan

HIGHLIGHTS

- The pH of TEMPOL electrolyte greatly affects the reversibility of its redox reaction.
- Reaction of TEMPOL with OH^- ion causes the decrease of electrolyte pH.
- TEMPOL in an acidic electrolyte leads to a decrease in its concentration.

GRAPHICAL ABSTRACT

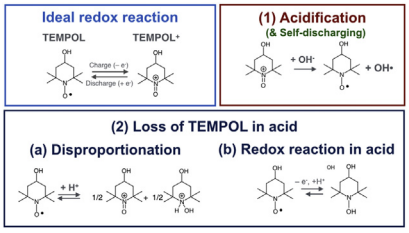

ARTICLE INFO

Article history:
Received 11 February 2016
Received in revised form
27 April 2016
Accepted 30 April 2016
Available online 6 May 2016

Keywords:
Flow battery
Aqueous battery
Radical compound
TEMPOL
Zinc anode

ABSTRACT

Electrochemical and UV-VIS measurements demonstrate that the pH value of a 4-hydroxy-2,2,6,6-tetramethyl-1-pipperidinyloxyl (TEMPOL) electrolyte significantly impacts its redox reversibility. The diffusion coefficient and kinetic rate constant of TEMPOL in neutral aqueous solution are determined and shown to be comparable to those of vanadium ions used for industrially utilized redox flow batteries (RFBs). RFBs that incorporate a TEMPOL catholyte and Zn-based anolyte have an average voltage of 1.46 V and an energy efficiency of 80.4% during the initial cycle, when subject to a constant current of 10 mA cm^{-2}. We demonstrate several factors that significantly influence the concentration and capacity retention of TEMPOL upon cycling; namely, pH and atmospheric gases dissolved in electrolyte. We expand upon the known reactions of TEMPOL in aqueous electrolyte and propose several concepts to improve its electrochemical performance in a RFB. Controlling these factors will be the key to enable the successful implementation of this relatively inexpensive and environmentally friendly battery.

1. Introduction

Redox flow batteries (RFBs) have attracted much attention for use in large-scale energy storage applications, such as in smart grids, because of their many advantages, including their flexible and modular design, as well as fast response time [1–4]. Typical RFBs comprise two electrolyte tanks for storing energy, a cell unit for converting energy, and pumps for circulating each electrolyte (catholyte and anolyte). This unique energy storage system enables the use of many kinds of materials, ranging from inorganic compounds such as vanadium [5], chromium [6], iron [7], bromine [8], and iodine [9,10], to organic compounds like quinone [11] and polysulfide [12]. These RFBs can be subdivided into two types: ones aimed at achieving high-energy density, and others designed for low cost and safety. The former type of batteries, including Li/I [10] and Li/polysulfide [12], are based on high voltages, which result from the low redox potential of Li metal. A myriad of problems involving lithium metal dendrites have yet to be solved, however,

* Corresponding author.
E-mail address: shmeng@ucsd.edu (Y.S. Meng).

http://dx.doi.org/10.1016/j.jpowsour.2016.04.136
0378-7753/

making the long-term stability of these systems challenging [13]. The latter group of batteries, such as anthraquinone-2,7-disulfonic acid/bromine [11], 2,6-dihydroxyanthraquinone/ferrocyanide [14], and zinc/iodine (Zn/I) [9] are suitable for grid-scale energy storage due to their inherently robust and safe systems. Although some of these aqueous batteries have issues, including the use of toxic bromine, strong alkaline electrolyte, and the formation of Zn dendrites, their cost effective materials and nonflammable electrolytes are definite benefits for grid-scale energy storage.

Recently, an inexpensive cathode material referred to as 2,2,6,6-tetramethylpiperidine-1-oxyl (TEMPO) has been explored for use in organic-based electrolytes [15,16]. Its performance when coupled with Li-ion anode is reasonably impressive, with a high energy density of 126 W h L^{-1} [15]. Interestingly, functionalizing the 4-position of TEMPO with a hydroxyl group results in relatively high solubility in water. The functionalized compound, referred to as TEMPOL (4-hydroxy-2,2,6,6-tetramethylpiperidine-1-oxyl), can be dissolved at concentration as high as 3.6 M. In addition, it bears the same sterically protected radical center associated with the delocalized unpaired electron of the N–O bond found in TEMPO [17–19]. For these reasons, TEMPOL may be a promising candidate for use as catholyte in an aqueous redox flow battery of high energy density. Previously, TEMPOL had been studied as catalyst [20], fluorescent probe [21], and electrode modifier in dye-sensitized solar cells [17]. Very recently, its feasibility for use as an electrolyte active material in RFBs has also been explored [22]. The TEMPOL/methylviologen system exhibited slight capacity decay over the course of 100 cycles, especially at high TEMPOL concentrations, but initial performance results were promising. Because the capacity fading mechanism is still unclear, this paper aims to elucidate aspects of the degradation that may arise from aqueous TEMPOL catholyte. The full range of optimized conditions, such as electrolyte pH and supporting electrolyte, have not yet been reported. The existence of side reactions in aqueous TEMPOL electrolyte has also not yet been thoroughly explored.

Nitroxyl radical compounds are known to have complex side reactions in H_2O, besides the ideal and reversible redox reaction observed in TEMPO [23,24]. As shown in Fig. 1, we hypothesize that TEMPOL mirrors the redox reaction of TEMPO both chemically and electrochemically; both the redox and known disproportionation reactions based on TEMPO are shown. Based on these mechanisms we propose that side reactions occur and are influenced by the pH of TEMPOL electrolyte. The effect of pH on the reversibility, diffusion coefficient, and kinetic rate constant of TEMPOL were examined in this study.

We report upon a new aqueous RFB using TEMPOL catholyte and zinc-based anolyte. These aqueous electrolytes can be used without any toxic or corrosive compounds under neutral conditions, and they are also inexpensive. The redox reactions of TEMPOL and the overall reaction of TEMPOL/Zn are shown in (1) and (2).

$$\text{TEMPOL} \rightleftarrows \text{TEMPOL}^{+} + e^{-} \quad E_{1/2} = 0.61 \text{ V vs. Ag/AgCl} \tag{1}$$

$$2\ \text{TEMPOL} + Zn^{2+} \rightleftarrows 2\ \text{TEMPOL}^{+} + \text{Zn} \quad E = 1.59 \text{ V} \tag{2}$$

The effects of both the supporting electrolyte and the separator on battery performance were analyzed. The supporting electrolytes were chosen among NaCl, Na_2SO_4, and $NaClO_4$ – all inexpensive, earth-abundant and relatively safe materials. In addition to Nafion, a hydrocarbon-type anion-exchange membrane (AEM) was tested as a separator. This separator is potentially less expensive than Nafion, a perfluorinated cation-exchange membrane (CEM) that has been commonly used in RFBs because of its high chemical stability [25].

2. Experimental

2.1. Materials

All chemicals, except Nafion, were used as received without any further purification. 4-Hydroxy-2,2,6,6-tetramethylpiperidine 1-oxyl (TEMPOL), sodium sulfate, sulfuric acid, zinc acetate dihydrate, and Nafion 212 were purchased from Sigma-Aldrich. Sodium perchlorate was purchased from EMD Millipore, and sodium

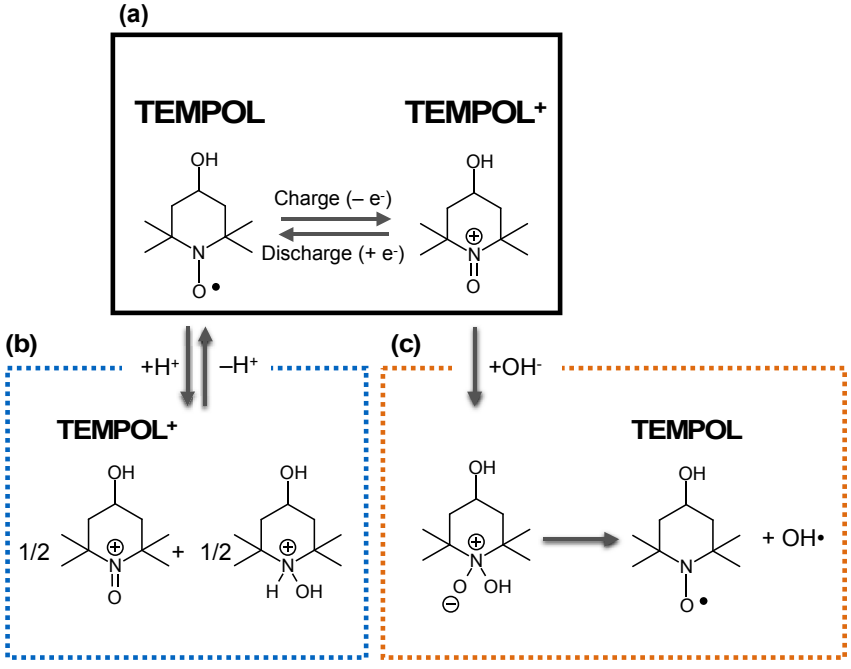

Fig. 1. (a) The ideal redox reaction of TEMPOL, (b) the disproportionation reaction of TEMPOL with H^+, and (c) the chemical reduction of $TEMPOL^+$ with OH^-.

chloride from Lab Chem. The pH of each solution was adjusted using sulfuric acid, sodium hydroxide, and pH 4, pH 7, and pH 10 buffer solutions. The pH value of each electrolyte was measured with an Oakton pH meter (pH-2700). Nafion212 (thickness: 50.8 μm) and SELEMION DSV (Asahi Glass, counter ion: Cl^-, thickness: 95 μm) were used as a CEM and AEM, respectively.

2.2. Full cell performance

The flow cell tests were carried out using an Arbin BT-2000 battery tester (Arbin Instruments) at 298 K. A lab-made flow cell was assembled with two graphite end plates, two Cu current collectors, two graphite felts (GEN ATOMIC-001, Midland materials research) and an exchange membrane as separator. Zinc foil was set on one graphite end plate as anode. Each 50 mL of catholyte and anolyte was flowed at a rate of 20 mL min^{-1} through a peristaltic pump. The active areas of the electrode and the separator were 36 cm^2. The graphite end plates did not have any flow channel. Nafion 212 was used after a treatment for exchanging H^+ with Na^+. This exchange procedure was carried out in 1 M NaOH at 80 °C for 6 h, followed by washing with deionized water several times, as according to previous literature [26].

Cycling of batteries was conducted at a constant current of 10 mA cm^{-2} (360 mA) between 1.0 V and 2.0 V. The electrochemical performances of batteries were evaluated according to three main criteria: (1) coulombic efficiency (CE), the ratio of the average discharge capacity to the average charge capacity; (2) voltaic efficiency (VE), the ratio of the average discharge voltage to the average charge voltage; and (3) energetic efficiency (EE), the average discharge energy to the average charge energy. Open circuit voltage (OCV) was measured after the initial charge process.

Two TEMPOL/Zn compositions were primarily explored: the first was 0.1 M TEMPOL in 1.0 M $NaClO_4$ aqueous catholyte and 0.3 M Zn acetate in 0.6 M NaCl aqueous anolyte; the second was 1.0 M TEMPOL in 3.0 M $NaClO_4$ catholyte and 1.0 M Zn acetate in 2.0 M NaCl anolyte. NaCl and Na_2SO_4 were also explored as supporting electrolytes for the catholyte.

To explore cycling at various SOC, testing was also conducted at a current density of 10 mA cm^{-2}, with fixed charge times. Those times were 2.3 min (SOC: 10%, capacity: 13.4 mAh, 0.134 A h L^{-1}) for RFBs using 0.1 M TEMPOL or 22.3 min (SOC: 10%, capacity: 134 mAh, 1.34 A h L^{-1}) for RFBs using 1.0 M TEMPOL. Each used 50 mL of catholyte and anolyte.

2.3. Voltammetry

Cyclic voltammetry (CV) and RDE experiments were conducted using an Arbin BT-2000 battery tester (Arbin Instrument) as well as a BASi RDE-2 with a BASi Ag/AgCl aqueous reference electrode (RE-5B, MF-2079, 3 M NaCl filling solution), platinum wire auxiliary counter electrode (MW-1033, 0.5 mm diameter), and glassy carbon working electrode (MF-2066, 3 mm diameter). The glassy carbon electrode was polished with 0.07 mm Alumina (CF-1050) and washed with deionized water. CV was conducted at various sweep rates between 0 V and 1.0 V vs. Ag/AgCl in 3 M NaCl aqueous electrolyte. CV and RDE were measured after deaerating the electrolyte with N_2 gas.

The half-wave potential $E_{1/2}$ was calculated as the average of the cathodic and anodic peak potentials. The formal redox potential $E^{0'}$ was replaced by the half-wave potential on the assumption that the diffusion coefficients of TEMPOL and $TEMPOL^+$ were identical. The peak separation was calculated from the potential difference between the cathodic and anodic peaks, at a sweep rate of 10 mV s^{-1}. The anodic maximum current (I_{pa}) was plotted versus the square root of the sweep rate, and the diffusion coefficient was calculated from the resulting fitted line according to the Randles-Sevcik equation [27]:

$$I_{pa} = 2.686 \times 10^5 \times n^{3/2} A c v^{1/2} D^{1/2}, \quad (5)$$

where n is the number of electrons gained in the reduction, A is the surface area of the working electrode (0.071 cm^2), D is the diffusion coefficient in $cm^2\ s^{-1}$, c is molar concentration in mol cm^{-3}, and v is sweep rate in V s^{-1}.

For RDE experiments, the current was measured from 0.4 V to 1.0 V vs. Ag/AgCl at a 5 mV s^{-1} sweep rate, during which time the electrode was rotated at 200–3000 rpm. The limiting currents measured at 1.0 V were plotted versus the rotation rate (ω). The slope was fit to the Levich equation [28]:

$$i = 0.620\ nFAcD^{2/3}\nu^{-1/6}\omega^{1/2}, \quad (6)$$

where i is the limiting current, F is the Faraday constant (96485 C mol^{-1}), ν is the kinetic viscosity in $cm^2\ s^{-1}$, and ω is the rotating angular velocity in rad s^{-1}. The current measured at each potential was plotted versus the square root of the electrode rotation rate. The resulting fitted line was expressed by the Koutecký-Levich equation [28]:

$$1/i = 1/i_k + 1/0.620\ nFAcD^{2/3}\nu^{-1/6}\omega^{1/2}, \quad (7)$$

where i_k is the heterogeneous rate constant. $\log_{10}(i_k)$, as calculated from the vertical-axis intercepts at each potential, was plotted versus the over potential (η), which was calculated from the difference between the measured potential and $E^{0'}$ for the TEMPOL/$TEMPOL^+$ couple. The fitted line was expressed by the Tafel equation [28]:

$$\log_{10}(i) = \log_{10}(i_0) + \alpha nF\eta/RT, \quad (8)$$

where i_0 is the exchange current in amp, α is the transfer coefficient, R is the universal gas constant (8.314 J K^{-1} mol^{-1}), and T is temperature (298 K). The exchange current i_0 was determined from the vertical-intercept, and the kinetic rate constant k_0 (cm s^{-1}) was calculated using the equation:

$$k_0 = i_0/nFcA, \quad (9)$$

where the concentrations of TEMPOL and $TEMPOL^+$ are meant to be the same.

2.4. Electrochemical impedance spectroscopy

Electrochemical impedance spectroscopy (EIS) was performed using a Solartron 1287 system coupled with a Solartron 1260 frequency response analyzer. The full-cells of TEMPOL/Zn were analyzed using EIS after electrolytes were pumped in and stopped. The EIS was measured over a frequency range of 500 kHz to 0.1 Hz with an applied ac voltage of 10 mV. The bulk electrolyte resistance was measured at the high-frequency intercept of the real axis.

2.5. UV-VIS spectroscopy

UV-VIS spectra were measured using a UV-VIS spectrometer UV-1800 (Shimadzu Scientific Instrument) with a slit width of 1.0 nm, and quartz spectrophotometer cell (Aldrich, 10 mm of optical path length). The spectrum was measured at a wavelength range of 300–800 nm at a sampling interval of 0.5 nm.

3. Results and discussion

3.1. Electrochemistry of TEMPOL

3.1.1. Effect of pH

Kinetic studies of aqueous TEMPOL solutions containing acidic, neutral, and basic supporting electrolytes were examined using CV and RDE. Fig. 2 shows the CV curves of TEMPOL electrolytes with pHs ranging from 1.1 to 12.6, in the presence of 1 M $NaClO_4$ as a neutral supporting electrolyte. More regarding the choice of supporting electrolyte is discussed later. CV was measured from a starting voltage of 0 V vs. Ag/AgCl. As seen in Fig. 2, the pH value strongly affected the shape of the CV curves. An ideal CV curve exhibiting a single reversible peak was obtained when the electrolyte pH was 4.2 or 6.7. The half-wave potential of the TEMPOL/$TEMPOL^+$ redox couple at near neutral conditions was 0.61 V vs. Ag/AgCl (0.83 V SHE). The peak separation was 73 mV at a sweep rate of 10 mV s^{-1}, which was close to the theoretical value of 57 mV expected of a one-electron reaction.

When using a strongly acidic electrolyte of pH 1.1, a large negative current was observed at the beginning of the CV measurements (0 V vs. Ag/AgCl). The overall CV curve was also shifted down towards negative current. This shift may be explained by the fact that TEMPOL can react with H^+ to chemically form the oxoammonium cation ($TEMPOL^+$) through disproportionation in acid, as shown in Fig. 1b [23,24]. In other words, $TEMPOL^+$ may be chemically formed in an acidic environment before any electrochemical charging occurs. The initial presence of $TEMPOL^+$ results in its immediate reduction. It should be noted that even at a weakly acidic condition (pH of 4.2) the slight negative current can be seen at 0 V vs. Ag/AgCl. The presence of TEMPOL and $TEMPOL^+$ can be distinguished by a difference in their absorptivities. We therefore performed UV-VIS spectroscopy to lend support to our hypothesis. Fig. 3 displays the UV-VIS spectra of 0.1 M TEMPOL in 1 M $NaClO_4$ aqueous solution at pHs of 1.1, 6.7, and 12.6. It can be seen that electrolyte pH strongly altered the UV-VIS spectra. A single absorption peak is observed at 425 nm for catholytes with pHs of 6.7 and 12.6. In a strongly acidic environment (pH 1.1), an additional absorption peak appeared at 477 nm. These peak positions are nearly identical to those of TEMPO and $TEMPO^+$, despite those materials' lack of 4-hydroxy functional groups [22]. We therefore assign the peaks at 425 and 477 nm to TEMPOL, and $TEMPOL^+$, respectively. Furthermore, these results suggest that $TEMPOL^+$ can form in acidic conditions, without imposing a charging current or bias. The molar extinction coefficient of TEMPOL was calculated to be 12.9 L mol^{-1} cm^{-1} from the absorptions of aqueous solutions containing various concentrations of TEMPOL (as shown in Fig. S1 in the Supplementary data).

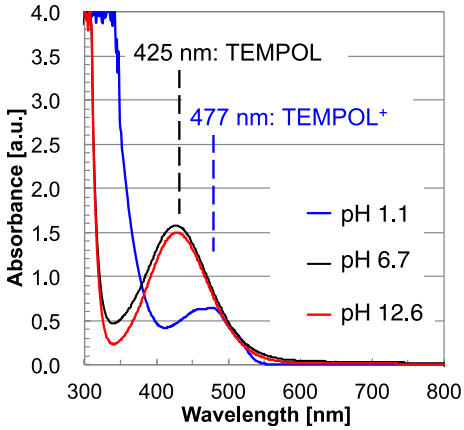

Fig. 3. UV-VIS spectra of 0.1 M TEMPOL in 1 M $NaClO_4$ aqueous solutions, at pHs of 1.1, 6.7, and 12.6.

In contrast to the aforementioned acid-induced shift towards negative current, the CV curve of a strongly basic TEMPOL electrolyte (pH of 12.6) exhibited only positive current. This may be explained by the fact that at a high OH^- concentration, $TEMPOL^+$ can be chemically converted back to TEMPOL as shown in Fig. 1c. As a result, the overall redox reaction of TEMPOL is irreversible in a strongly basic electrolyte. The positive current shift in the CV curve was observed even in a weakly basic electrolyte (pH of 9.6), indicating that TEMPOL should be used in near-neutral aqueous electrolyte to avoid side reactions, particularly the disproportionation and chemical reduction mechanisms described in Fig. 1b and c.

3.1.2. Kinetic rate constant

To expand upon the kinetics and in particular the diffusion of TEMPOL in aqueous electrolyte, we analyzed the dependence of the peak current on CV scan rate. Fig. 4a shows the CVs of 0.1 M TEMPOL in a 1 M $NaClO_4$ electrolyte (pH 6.7) at scan rates ranging from 10 to 200 mV s^{-1}. The inset of Fig. 4a displays the dependence of the anodic peak current (I_{pa}) on scan rate. The resulting trend line has good linearization and passes through the origin, demonstrating that the redox reaction of TEMPOL was controlled by diffusion. Using the slope of the trend line in the inset of Fig. 4a and the Randles-Sevcik equation (Eq. (5)), the diffusion rate of TEMPOL was calculated to be 2.2 × 10^{-6} cm^2 s^{-1}. To compare, the diffusion

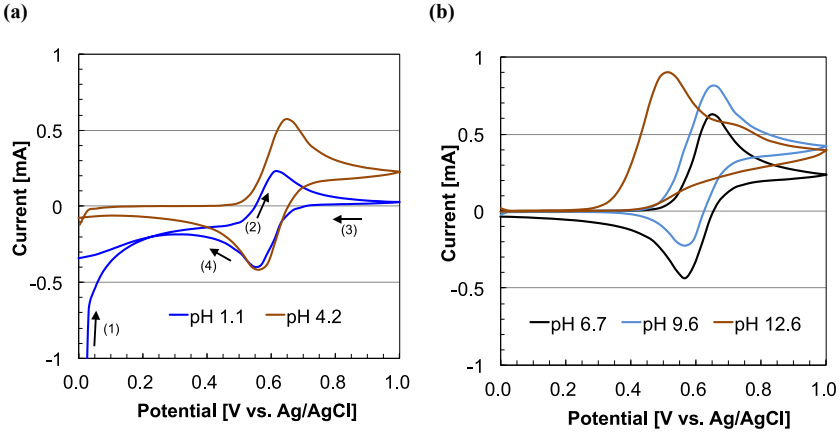

Fig. 2. CVs of 0.1 M TEMPOL in 1 M $NaClO_4$ catholytes with various pHs, ranging from 1.1 to 12.6, at a scan rate of 25 mV s^{-1} vs. Ag/AgCl. (a) pH 1.1 and 4.2. (b) pH 6.7, 9.6, and 12.6.

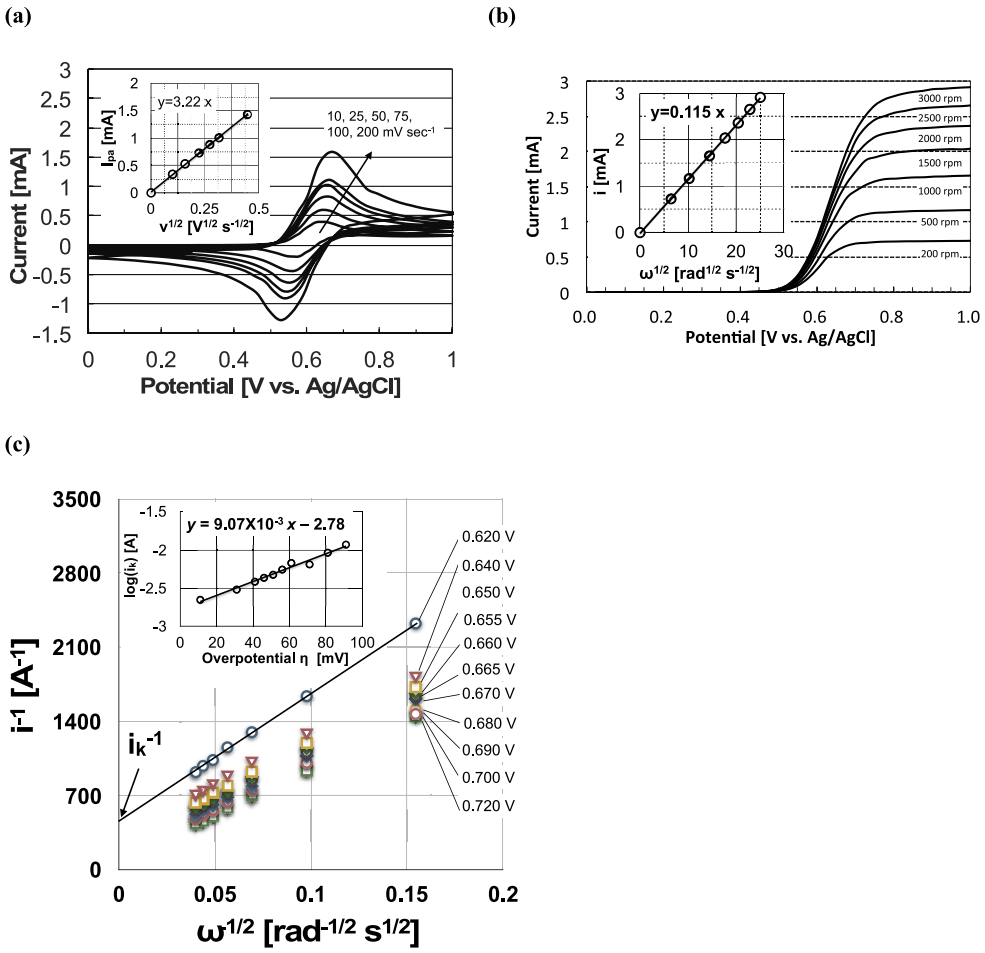

Fig. 4. Electrochemistry of 0.1 M TEMPOL in 1 M $NaClO_4$ catholyte (pH = 6.7): (a) CVs at sweep rates from 10 to 200 mV s^{-1}; inset shows the anodic peak current (I_{pa}) vs. the square root of sweep rate; (b) RDE measurements at rotating electrode speeds from 200 to 3000 rpm; inset shows the limiting current (i) vs. the square root of the rotation velocity (Levich-plot); (c) Koutecký-Levich plot and Tafel plot in the inset.

rates of other popular flow battery alternatives, such as V^{3+} and Fe^{3+}, are 1.5×10^{-6} and 6.0×10^{-6} cm^2 s^{-1}, respectively [2].

To complement CV, the diffusion coefficient and kinetic rate constant were investigated using RDE. Fig. 4b shows the limiting diffusion current at various rotating angular velocities of the RDE. The inset of Fig. 4b displays the dependence of the limiting current on rotating velocity using 0.1 M TEMPOL in a 1 M $NaClO_4$ electrolyte. The fact that the linear trend line crosses the origin means that there was no observed chemical reaction that preceded or followed the redox reaction of TEMPOL/$TEMPOL^+$ under neutral conditions, in the time frame used within the experiment. The diffusion coefficient of TEMPOL was determined to be 1.3×10^{-6} cm^2 s^{-1} using the Levich equation (Eq. (6)).

Fig. 4c shows a Koutecký-Levich plot, which provides the heterogeneous rate constant i_k at each potential (Eq. (7)). i_k represents the current in the absence of any mass-transport effects. These values were used to create the Tafel plot shown in the inset of Fig. 4c, which in turn was used to determine the exchange current density (Eq. (8)) – $i_0 = 2.34 \times 10^{-2}$ A cm^{-2} – at the equilibrium potential. The transfer coefficient for the oxidation of TEMPOL was also calculated from this plot to be $\alpha = 0.54$. This value is close to the value of 0.5, obtained for a reaction in which the energy barriers for oxidation and reduction are symmetric [28]. From Eq. (9), the kinetic rate constant of TEMPOL at the equilibrium potential was found to be $k_0 = 2.4 \times 10^{-3}$ cm^2 s^{-1}, which is comparable to those of polymer bearing TEMPO/$TEMPO^+$ (4.5×10^{-4} cm s^{-1}) [16], V^{3+}/V^{2+} (5.3×10^{-4} cm s^{-1}) [29], VO^{2+}/VO_2^+ (2.8×10^{-6} cm s^{-1}) [29], redox couples of 9,10-anthraquinone-2,7-disulphonic acid (7.3×10^{-3} - cm s^{-1}) [9], and Fe^{2+}/Fe^{3+} (2×10^{-5} cm s^{-1}) [30]. According to Matsuda's equation, the kinetic rate constant of TEMPOL can be classified as a quasi-reversible reaction [31]. More detail regarding this classification can be found in the Supporting Information.

3.2. Full-cell performance of TEMPOL/Zn RFBs

3.2.1. Separator and supporting electrolyte

Full-cell testing of TEMPOL/Zn RFB with 0.1 M TEMPOL was conducted using a constant current of 10 mA cm^{-2} between 1.0 V and 2.0 V. The separator used was either a CEM (Nafion) or an AEM (SELEMION), and the supporting electrolyte was either 1 M $NaClO_4$ or 1 M NaCl. Nafion was used after a treatment that exchanged H^+ with Na^+, to avoid acidification of the TEMPOL electrolyte. The initial charge-discharge profiles of RFBs using various combinations of these materials are shown in Fig. 5a and Fig. 5b. When using a CEM separator, a distinct inflection point in the discharge curve was observed, which resulted in the lower voltage plateau around 1.3 V (Fig. 5a). It has been reported that vanadium ions show affinity with the SO_3^- groups in Nafion membranes [32,33]. For vanadium RFBs, it is recommended to use anion exchange membranes so that the interaction between the vanadium ions and separator can be suppressed [34]. For TEMPOL-based RFBs, the two-stage discharge curve may likewise be caused by the chemical reaction of $TEMPOL^+$

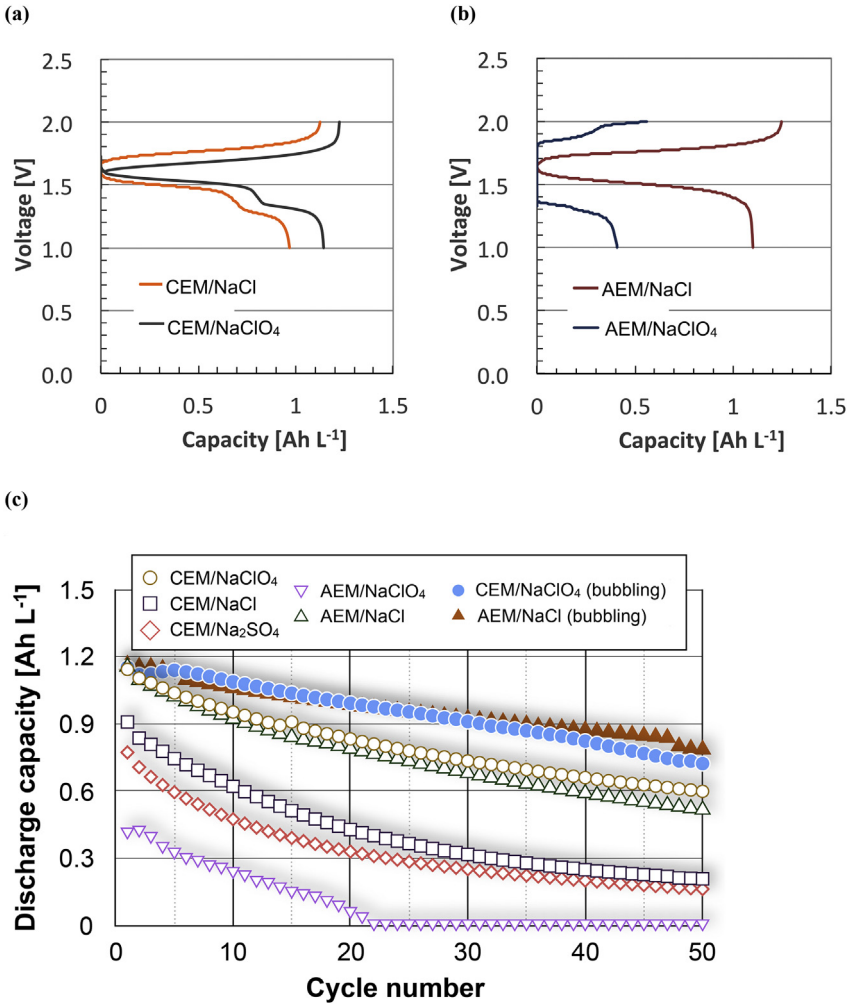

Fig. 5. Cycling of TEMPOL/Zn RFBs using 0.1 M supporting electrolyte. 1st cycle voltage curves from constant current charge/discharge at 10 mA cm^{-2}, using (a) a CEM and (b) an AEM; (c) discharge capacities over 50 cycles.

with the CEM. Unreacted $TEMPOL^+$ may discharge at the typical voltage of 1.5 V, while $TEMPOL^+$ reacted with SO_3^- groups of the CEM may discharge at the lower 1.3 V.

Table 1 summarizes the initial full-cell performance of TEMPOL/Zn RFBs at 10 mA cm^{-2}. The TEMPOL/Zn RFB with CEM and $NaClO_4$ showed the highest initial efficiencies (CE of 93.4%, VE of 86.1%, and EE of 80.4%) and an average discharge voltage of 1.46 V. The combination of CEM and $NaClO_4$ likely performed well because the water-solubility of $NaClO_4$ is higher than NaCl and typically suppresses the precipitation of solutes, such as those formed from TEMPOL, due to the weaker basicity of ClO^{4-} than Cl^- and SO_4^{2-}. Indeed, at high TEMPOL concentrations, precipitates regularly form over time when using NaCl supporting electrolyte and do not when using $NaClO_4$ (i. e. 1 M TEMPOL and 3 M supporting electrolyte). The performance of $NaClO_4$ with an AEM is worse because $NaClO_4$ oxidizes AEMs. When using an AEM, therefore, NaCl supporting electrolyte is required. The fact that the AEM was thicker than the CEM may explain why RFBs with an AEM and NaCl showed lower efficiencies than those with CEM and $NaClO_4$. To validate this hypothesis, bulk electrolyte resistances were measured using electrochemical impedance spectroscopy (EIS). Table 1 compares the bulk electrolyte resistances of RFBs using either a CEM or AEM and NaCl or $NaClO_4$ supporting electrolytes, while Fig. S2 illustrates their Nyquist plots. The use of an AEM showed bulk resistances two times as large as a CEM, indicating that the AEM led to lower ionic conductivities.

Fig. 5c displays the cycling discharge capacities of TEMPOL/Zn RFBs with the various combinations of separators and supporting electrolytes. While the identity of supporting electrolyte showed no clear effect in CV measurements (Fig. S3), it strongly affected the

Table 1
The initial full-cell performances of TEMPOL/Zn RFBs at a current density of 10 mA cm^{-2} and bulk electrolyte resistances R_b. The concentrations of TEMPOL and the supporting electrolyte were 0.1 M and 1.0 M, respectively.

Separator	Supporting electrolyte	OCV after charge [V]	Average discharge voltage [V]	CE [%]	VE [%]	EE [%]	R_b [Ω]
CEM	$NaClO_4$	1.73	1.46	93.4	86.1	80.4	0.18
CEM	NaCl	1.73	1.42	86.1	79.9	68.8	0.19
AEM	$NaClO_4$	1.62	1.29	73.4	67.1	49.3	0.39
AEM	NaCl	1.74	1.49	88.3	83.9	74.0	0.39

cycling performances of the RFBs. Among the various combinations of membrane and supporting electrolyte, the use of a CEM with $NaClO_4$ supporting electrolyte showed the highest capacity retention, at 51% after 50 cycles. Fig. 6a and Fig. 6b highlight the voltage curves and efficiencies of the TEMPOL/Zn RFB with CEM and $NaClO_4$ over 50 cycles. Based upon the charge and discharge curves, the capacity from the low voltage plateau decreases at a disproportionately higher rate. This may suggest that the $TEMPOL^+$ that reacted with the CEM is not stable. While the RFB with AEM and NaCl demonstrated a more stable discharge profile, as shown in Fig 6c and Fig. 6d, its overall capacity retention was slightly lower (45%). The overall concentration of TEMPOL after 50 cycles with a CEM and $NaClO_4$ was calculated to be 58 mM and 52 mM from UV-VIS and CV measurements, respectively (Fig. S4). These TEMPOL concentration retentions (58% and 52%) are close to the electrochemical capacity retention (51%). No TEMPOL or $TEMPOL^+$ was observed in the UV-VIS spectrum of the anolyte after 50 cycles, indicating that TEMPOL did not cross over from the catholyte to the anolyte in either the CEM or AEM. Zn^{2+} ion could also not be detected from the CVs of catholyte after cycling, indicating that the crossover of Zn^{2+} ions is negligible. After 50 cycles the pH of the catholyte also decreased from 6.7 to 4.0. This pH change may have been caused by the consumption of OH^- ions in the reaction of $TEMPOL^+$, as shown in Fig. 1c. This can lead to two issues: 1) the hydroxyl radical formed in this process may further react to decompose TEMPOL; 2) following the decrease in pH, TEMPOL can undergo the disproportionation reaction shown in Fig. 1b. In addition, TEMPOL may also undergo redox with H^+ to form 1,4-dihydroxy-2,2,6,6-tetramethylpiperidine through the reactions shown in Fig. S5. In both cases, the reactions of TEMPOL with H^+ and hydroxyl radical can lead to a decrease in the concentration of TEMPOL. The less than 100% Coulombic efficiency (98%) may be explained by the chemical reduction of $TEMPOL^+$ with OH^-.

3.2.2. Bubbling of electrolyte

Dissolved CO_2 in aqueous electrolyte may affect pH, as shown in Eq. (10) and Eq. (11), by releasing H^+ into the electrolyte.

$$CO_2 + H_2O \rightleftarrows H^+ + HCO_3^- \quad pK_{a1} = 6.35 \tag{10}$$

$$HCO_3^- \rightleftarrows H^+ + CO_3^{2-} \quad pK_{a2} = 10.33 \tag{11}$$

In addition, dissolved O_2 may act as an oxidizing agent to remove an electron from TEMPOL, which would affect battery performance. To mitigate this and possibly other effects associated with exposure to air [16,22], the effect of air removal from electrolytes was examined. Fig. 5c shows the cycling discharge capacities of TEMPOL/Zn RFBs with CEM/$NaClO_4$ and AEM/NaCl when subject to N_2-bubbling. Fig. S6a and b show that the voltage profiles did not appreciably differ from the non-bubbled condition; however, its overall capacity retention after 50 cycles was improved from that of the non-bubbled system. While the mitigation of dissolved gases, such as CO_2 and O_2, improved retention, it did not entirely eliminate capacity fading. The catholyte pH still decreased from 6.7 to 4.3, and the TEMPOL concentration also decreased to 68 mM after 50 cycles. Though slight improvements in concentration retention and pH resulted from elimination of air, because those two factors still decreased significantly, we propose that the aforementioned side reactions of TEMPOL and $TEMPOL^+$ results in the primary degradation mechanisms.

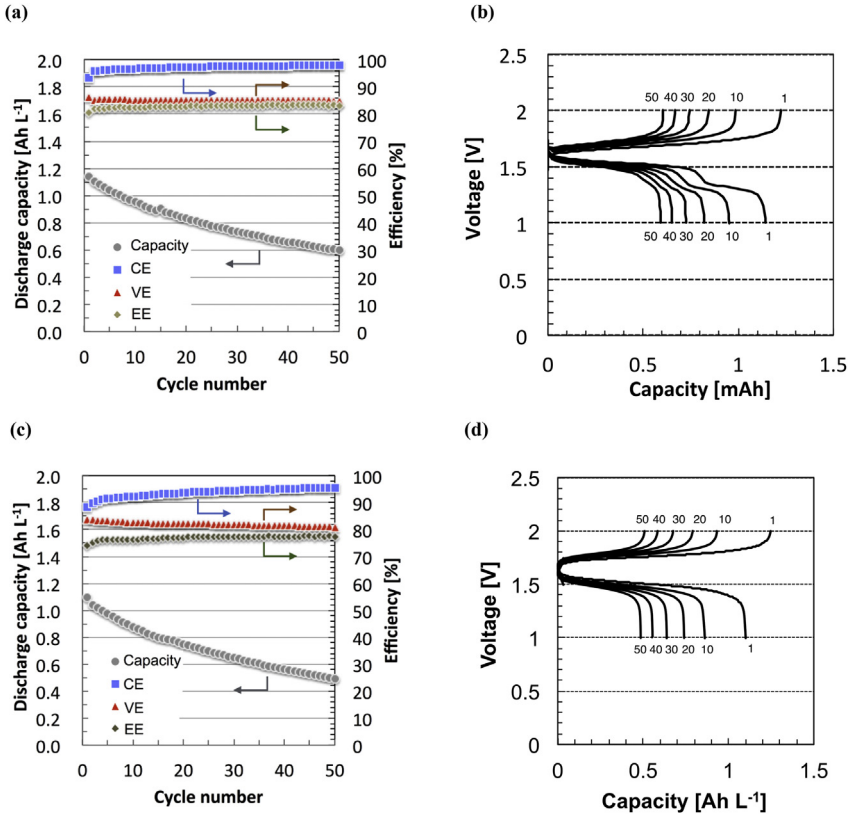

Fig. 6. Electrochemical performances of RFBs using a CEM (a,b) and an AEM (c,d). Electrolytes consist of 0.1 M TEMPOL ((a, b) 1 M $NaClO_4$, (c, d) 1 M NaCl) catholyte and 0.3 M Zn acetate (0.6 M NaCl) anolyte. (a,c) represent discharge capacities and efficiencies over 50 cycles; (b,d) represent their voltage curves at the 1st, 10th, 20th, 30th, 40th, and 50th cycles.

3.2.3. TEMPOL concentration and degradation rate

A high concentration of TEMPOL is predicted to accelerate a pH change upon cycling because high TEMPOL concentrations increase the reaction rate between $TEMPOL^+$ and OH^-. The reaction rate of $TEMPOL^+$ with OH^- is proportional to their concentrations, as shown by Eq. (12).

$$d[OH^-]/dt = -k\,[TEMPOL^+][OH^-] \quad (12)$$

The charge-discharge profiles of the high-TEMPOL-concentration RFB with 1 M TEMPOL are shown in Fig. 7a. At concentrations higher than 1.5 M TEMPOL (in 3 M $NaClO_4$), we observed precipitation to occur. The full-cell included 3 M $NaClO_4$ supporting catholyte, a CEM, and 1 M Zn acetate/2 M NaCl supporting anolyte. The initial CE, VE, and EE of the RFBs were 83.3%, 81.1%, and 67.5%, respectively, at 10 mA cm^{-2}. The measured capacity and energy densities were 8.0 A h L^{-1} and 9.6 W h L^{-1}. However, the capacity retention after only 5 cycles was down to near 0%, as shown in Fig. 7b. The catholyte pH also decreased from 6.6 to 3.3 after the 5 cycles. The high concentration of $TEMPOL^+$ may have caused greater consumption of OH^-, leading to an accelerated decrease in catholyte pH. The low Coulombic efficiency, which was less than 90%, may be explained by the chemical degradation of active material caused by the side reaction of $TEMPOL^+$ with OH^- ions. The reaction rate or equilibrium state of $TEMPOL^+$ with H^+ may have also been affected by the TEMPOL concentration. The above suggests that a TEMPOL-based aqueous system may have an inherent problem associated with side reaction related to H^+ and OH^-.

In an attempt to mitigate the side reactions promoted when using high TEMPOL concentrations, cycling was conducted between 0% and 10% SOC. The cycling life of a variety of conventional batteries and RFBs have been extended in this practical manner [35,36]. Fig. 8a shows the discharge capacities and efficiencies of a TEMPOL/Zn RFB using 0.1 M TEMPOL, an AEM, and NaCl supporting electrolyte over 800 cycles, without bubbling. The figure demonstrates that stable discharge capacities, CEs, VEs, and EEs can be obtained over this duration. A TEMPOL/CEM/Zn RBF with 1.0 M TEMPOL catholyte was also cycled at 10% SOC (Fig. 8b). At the higher concentration, no capacity decay was observed over 100 cycles, even though voltage efficiencies deteriorated gradually. The voltage curves of RFBs using 0.1 M TEMPOL and 1 M TEMPOL, shown in Fig. S7, demonstrate that the polarization between charge and discharge increased upon cycling, but the profiles did not change appreciably. Notably, the charge overpotentials at high TEMPOL concentrations (Fig. S7b) became significantly greater than

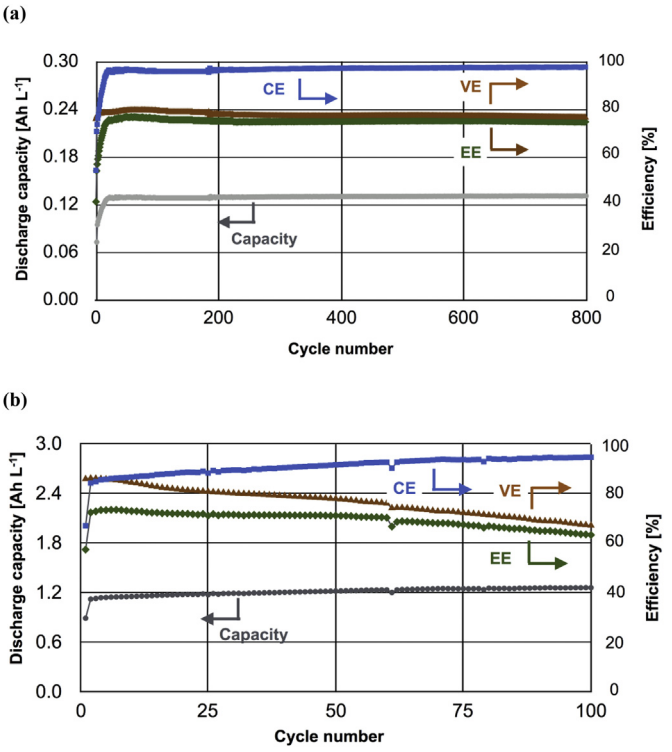

Fig. 8. (a) Discharge capacity, CE, VE, and EE over 800 cycles of a RFB using 0.1 M TEMPOL (1 M NaCl) catholyte, 0.3 M zinc acetate (1 M NaCl) anolyte, and an AEM at 10 mA cm^{-2}. (b) Discharge capacity, CE, VE, and EE over 100 cycles of a RFB using 1 M TEMPOL (3 M $NaClO_4$) catholyte, 1 M zinc acetate (2 M NaCl) anolyte, and a CEM at 10 mA cm^{-2}. Charge capacities were fixed to 0.134 A h L^{-1} and 1.34 A h L^{-1}, corresponding to 10% SOC, for RFBs using 0.1 M and 1.0 M TEMPOL, respectively.

discharge overpotentials. In addition, catholyte pHs after 100 cycles decreased from 6.6 to 4.5 when using 1 M TEMPOL catholyte. The drop in pH can improve the electrochemical reduction of $TEMPOL^+$ (as shown in Fig. 2a), which explains the increasing Coulombic efficiency over time. The reduced form of $TEMPOL^+$ in acidic conditions is not reversible, however, as described by the side reactions above (Fig. 1 and Fig. S5). The increasing charge overpotentials may therefore result from the large concentration gradient between TEMPOL and the non-oxidizable side reaction products formed. While cycling at low TEMPOL concentrations and limited SOC was shown to dramatically improve cycle life, the fundamental issue of side reaction with OH^- and H^+ was still evident. Addressing how to

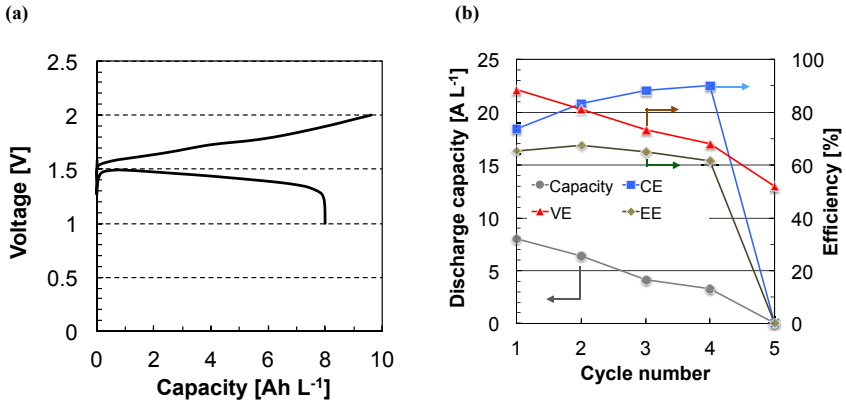

Fig. 7. Electrochemical performance of a RFB using 1 M TEMPOL (3 M $NaClO_4$) catholyte, 1 M Zn-acetate (2 M NaCl) anolyte, and a CEM at constant current of 10 mA cm^{-2}: (a) 1st cycle voltage profiles and (b) discharge capacity, CE, VE, and EE over 5 cycles.

circumvent this problem will be crucial for the further development of this material in RFBs.

4. Conclusions

This work provides much deeper insight to understand the side reactions concerning TEMPOL, in order to develop aqueous RFBs based on nitroxyl radical compounds. We have demonstrated the significant effect of pH on the electrochemical reversibility of TEMPOL/TEMPOL$^+$. CV showed that TEMPOL could be chemically charged by reaction with H^+ in an acidic electrolyte. It also showed that TEMPOL$^+$ could be chemically discharged by reaction with OH^- in a strongly basic electrolyte. RDE experiments showed that the redox reaction of TEMPOL in near-neutral conditions could be classified as a quasi-reversible reaction, and the kinetic rate constant of TEMPOL/TEMPOL$^+$ was greater than V^{3+}/V^{2+} (2.4×10^{-3} vs. 5.3×10^{-4} cm s^{-1}).

The capacity fade of TEMPOL-based RFBs corresponded to a decrease in TEMPOL concentration. In more detail: the catholyte pH decreased from neutral to weakly acidic during cycling, and the reversibility of TEMPOL deteriorated because of its side reactions in acid. The following two steps can explain this loss of TEMPOL: (1) OH^- ions reacted with TEMPOL$^+$ as a side reaction during cycling, and the consumption of OH^- ions made the catholyte acidic; (2) TEMPOL was consumed by reaction with H^+ to be converted to other compounds, such as 1,4-dihydroxy-2,2,6,6-tetramethylpiperidine. Dissolved CO_2 as a buffer and O_2 as an oxidant also affected the cycling performance of TEMPOL/Zn RFBs; the total capacity and retention over 50 cycles were greater when air was eliminated from the cell. Although RFBs using 1 M TEMPOL showed a relatively high energy density of 9.6 W h L^{-1}, the capacity decay was accelerated by high TEMPOL concentrations. Although further improvement is still necessary to make TEMPOL-based RFBs suitable for practical applications, this study demonstrates its feasibility with Zn-based anolytes and provides valuable insight into its deleterious side reactions.

Acknowledgement

The UCSD team acknowledges the funding from Advanced Research Projects Agency - Energy (ARPA-E) under Grant No. DE-AR0000520.

Appendix A. Supplementary data

Supplementary data related to this article can be found at http://dx.doi.org/10.1016/j.jpowsour.2016.04.136.

References

[1] C.P. Leon, A. Frias-Ferrer, J. Gonzalez-Garcia, D.A. Szanto, F.C. Walsh, J. Power Sources 160 (2006) 716–732.
[2] A.Z. Weber, M.M. Mench, J.P. Meyers, P.N. Ross, J.T. Gostick, Q. Liu, J. Appl. Electrochem. 41 (2011) 1137–1164.
[3] Q. Huang, Q. Wang, ChemPlusChem 80 (2015) 312–322.
[4] G.L. Soloveichik, Chem. Rev. 115 (2015) 11533–11558.
[5] A. Cunha, J. Martins, N. Rodrigues, F.P. Brito, Int. J. Energy Res. 39 (2015) 889–918.
[6] L. H. Thaller, NASA-TM-X-71540 (1974).
[7] L.W. Hruska, R.F. Savinell, J. Electrochem. Soc. 128 (1981) 18–25.
[8] F.C. Walsh, Pure Appl. Chem. 73 (2001) 1819–1837.
[9] B. Li, Z. Nie, M. Vijayakumar, G. Li, J. Liu, V. Sprenkle, W. Wang, Nat. Commun. 6 (2015) 6303.
[10] Y. Zhao, L. Wang, H.R. Byon, Nat. Commun. 4 (2012) 1896.
[11] B. Huskinson, M.P. Parshak, C. Suh, S. Er, M.R. Gerhardt, C.J. Galvin, X. Chen, A. Aspuru-Guzik, R.G. Gordon, M.J. Aziz, Nature 505 (2014) 195–198.
[12] Y. Yang, G. Zheng, Y. Cui, Energy Environ. Sci. 6 (2013) 1552–1558.
[13] W. Xu, J.L. Wang, F. Ding, X.L. Chen, E. Nasybutin, Y.H. Zhang, J.G. Zhang, Energy Environ. Sci. 7 (2014) 513–537.
[14] K. Lin, Q. Chen, M.R. Gerhardt, L. Tong, S.B. Kim, L. Eisenach, A.W. Valle, D. Hardee, R.G. Gordon, M.J. Aziz, M.P. Marshak, Science 349 (2015) 1529–1532.
[15] X. Wei, W. Xu, M. Vijayakumar, L. Cosimbescu, T. Liu, V. Sprenkle, W. Wang, Adv. Mater. 26 (2014) 7649–7653.
[16] T. Janoschka, N. Martin, U. Martin, C. Friebe, S. Morgenstern, H. Hiller, M.D. Hager, U.S. Schubert, Nature 527 (2015) 78–81.
[17] K. Nakahara, S. Iwasa, M. Satoh, Y. Morioka, J. Iriyama, M. Suguro, E. Hasegawa, Chem. Phys. Lett. 359 (2002) 351–354.
[18] R. Kato, F. Kato, K. Oyaizu, H. Nishide, Chem. Lett. 43 (2014) 480–482.
[19] K. Takechi, Y. Kato, Y. Hase, Adv. Mater. 27 (2015) 2501–2506.
[20] B. Han, C. Wang, R.-F. Han, W. Yu, X.-Y. Duan, R. Fang, X.-L. Yang, Chem. Commun. 47 (2011) 7818–7820.
[21] K. Żamojć, M. Zdrowowicz, W. Wiczk, D. Jacewicz, L. Chmurzyński, RSC Adv. 5 (2015) 63807–63812.
[22] T. Liu, X. Wei, Z. Nie, V. Sprenkle, W. Wei, Adv. Energy Mater. (2015) 1501449.
[23] V.D. Sen, V.A. Golubev, J. Phys, Org. Chem. 22 (2009) 138–143.
[24] Y. Ma, C. Loyns, P. Price, V. Chechik, Org. Biomol. Chem. 9 (2011) 5573–5578.
[25] V. Viswanathan, A. Crawford, D. Stephenson, S. Kim, W. Wang, B. Li, G. Coffey, E. Thomsen, G. Graff, P. Balducci, M. Kintner-Meyer, V. Sprenkle, J. Power Sources 286 (2014) 1040–1051.
[26] C. Cao, H. Wang, W. Liu, X. Liao, L. Li, Int. J. Hydrog. Energy 39 (2013) 16110–16115.
[27] K. Ngamchuea, S. Eloul, K. Tschulik, R.G. Compton, J. Solid State Electrochem. 18 (2014) 3251–3257.
[28] A.J. Bard, L.R. Faulkner, Electrochemical Methods: Fundamentals and Applications, second ed., John Wiley&Sons, New York, 2000 p.92, 99, 102, 339, and 341.
[29] T. Yamamura, N. Watanabe, T. Yano, Y. Shiokawa, J. Electrochem. Soc. 152 (2005) A830–A836.
[30] L.A. Curtiss, J.W. Halley, J. Hautman, N.C. Hung, Z. Nagy, Y.-J. Rhee, R.M. Yonco, J. Electrochem. Soc. 138 (1991) 2032–2040.
[31] H. Matsuda, A. Ayabe, Z. Elektrochem. 59 (1955) 494–503.
[32] S. Cui, S.J. Paddison, J. Phys. Chem. C 119 (2015) 12848–12855.
[33] H.-S. Cho, M. Ohashi, J.W.V. Zee, J. Power Sources 267 (2014) 547–552.
[34] J. Suna, X. Lia, X. Xia, Q. Laia, T. Liua, H. Zhang, J. Power Sources 271 (2014) 1–7.
[35] P. Zhao, H. Zhang, H. Zhou, B. Yi, Electrochim. Acta 51 (2005) 1091–1098.
[36] Y. Munaiah, S. Suresh, S. Dheenadayalan, V.K. Pillai, P. Ragupathy, J. Phys. Chem. C 118 (2014) 14795–14804.